Mercury: Industrial IBC Cell with Front Floating Emitter For 20.9% and Higher Efficiency

[1]Nicolas Guillevin, [1]Agnes Mewe, [1]Pierpaolo Spinelli, [1]Antonius Burgers, [1]Gaby Janssen, [2]Bas van de Loo, [2]Erwin Kessels, [3]Ard Vlooswijk, [1]Bart Geerligs, and [1]Ilkay Cesar

[1]ECN Solar Energy, Petten, NL-1755 LE, The Netherlands, [2]Eindhoven University of Technology, Eindhoven, NL-5612 AP, The Netherlands, [3]Tempress Systems, Vaassen, NL-8171 MD, The Netherlands

Abstract — This paper presents our recent progress in the development and characterization of our 6" industrial IBC Mercury cells. We gained more than 1% absolute in efficiency by optimizing the processes and design of the cells, resulting in 20.9% cell efficiency. Our cell process does not create a space or "gap" between the rear-side emitter and BSF areas, consequently the cells have a long length of high-high pn-junction on the rear side. We present a method to characterize the pn-junction recombination and quantify its contribution to Voc and pseudo-FF losses, one of the key performance parameters for optimisation of a gap-less IBC cell, and illustrate how this was central to the recent efficiency improvement. Together with these results, we briefly point out some key aspects of the design and production processes that ensure the industrial manufacturability of the cell and module. Finally, our roadmap towards >23% efficient Mercury cells is presented.

I.   INTRODUCTION

The recent International Technology Roadmap for PV report forecasts the rear-side contacted cell technology to gain a market share of at least 20% by 2025 [1]. This forecast is supported by market trends towards higher performance, lower costs/kWh, and by the interest in improved aesthetics of PV systems. In accordance with this trend, ECN develops an Interdigitated back contact (IBC) homo-junction solar cell, which differs from the well-known IBC cells with front surface field (FSF). Although IBC cells with a FSF have shown to yield very high conversion efficiencies, cost effective production of these devices poses challenges. To prevent performance losses due charge recombination above the back surface field (BSF) known as the electrical shading effect [2], the typical width of the BSF is reduced to the order of 0.2-0.4 mm, out of a typical cell pitch of 1.5 mm. The inequality of BSF and emitter widths results in the need for strict patterning tolerances in processing but also has implications for the metallization as shown in our previous publication [3]. To avoid the need for a narrow BSF width, the Mercury cell developed at ECN is an interdigitated back contact (IBC) cell which employs a conductive p$^+$-doped front floating emitter (FFE). A schematic cross-section of the Mercury cell is shown in Figure 1.
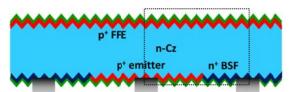

Fig. 1.   Schematic cross-section of a Mercury IBC cell. The dashed box indicates the unit cells used in device simulations.

The FFE enhances lateral transport properties for minority carriers (holes) at the front. In addition, it induces a "pumping effect" which transports holes from regions above the BSF to the rear emitter, limiting the effect of electrical shading of the BSF areas at the rear. With proper tuning of conductance and Jo, the FFE can be applied as an effective means to increase the BSF width with marginal loss in cell performance while assuring process simplification and cost reduction. The FFE benefits were described in more detail previously [3].

The development of FFE cells was reported recently by other research groups as well. Müller et al. [4] reported an attractive process flow for an FFE IBC cell that reached 21.7% on 2x2 cm based on P-implantation that selectively blocks the following BBr$_3$ diffusion. The screen printed 6 inch IBC cells that ISC Konstanz has reported [5] achieved 21.5% efficiency. These cells also feature a FFE, illustrating the potential of this low-cost approach.

In this paper, manufacturability aspects of the IBC Mercury technology are discussed, together with the latest results obtained. Then a characterisation method and results for the rear-side emitter-BSF pn-junction recombination are described. As illustration of the method, we monitor the impact of pn-junction recombination as a function of the boron diffusion recipe meant that creates the rear emitter and FFE, and we elaborate on the physical background to understand it. Finally, we discuss the work in progress and further process optimization possible for the Mercury IBC cells, part of our roadmap towards industrial IBC cells with efficiency over 23%.

II. MANUFACTURABILITY AND PERFORMANCE

The ECN IBC Mercury process technology remains close to our industrial n-Pasha process technology. The same process equipment as for n-Pasha is used in a similar number of process steps, with equipment as well as, importantly, process parameters, being compatible with an industrial scale production and throughput. Cells are processed on commercially available 156x156 mm2 n-Cz wafers. The cell structure comprises an interdigitated boron-doped emitter and a phosphorous-doped Back Surface Field (BSF) on the rear-side and a boron-doped FFE on the front-side. Doped regions are created by means of tube diffusion processes and are designed to be suitable for industrial throughput, i.e. lower cycle time and high load density. The FFE and the rear emitter are formed in a single Boron diffusion step and the recipe of this step is varied in this work to study the effect of pn-junction recombination. Structuring of the rear-side diffusions does not involve the creation of a gap between the emitter and the BSF. This patterning approach of diffusions greatly simplifies processing of the device and reduces manufacturing costs. Front-side and rear-side surface passivation and anti-reflecting coatings are applied by industrial ALD and PECVD equipment. The metallisation consists of a firing-through Ag paste deposited in a single step, for both emitter and BSF, by screen-printing and features an open grid design suitable for thin wafers and bifacial applications. The metallisation grid design includes busbars and 62 interconnections pads as shown in figure 2.

Fig 2 . Rear-side grid design of the IBC Mercury cell.

It is of importance to note that the busbars and interconnection points in this design are directly printed and contacted to the cell by fire-through metal paste, just as the fingers. Consequently, the relatively wide metal busbar areas inherently contact wide busbar diffusion areas. Due to the mitigating pumping effect the wider (BSF) diffusion areas will cause only a minor electrical shading loss in the I_{sc} of the cell. Based on this design, the cells can be readily processed into modules thanks to ECN's foil-based interconnection design [6] and does not require multi-level metallisation involving an isolation layer.

The ECN module manufacturing technology used to interconnect the IBC Mercury cells is based on an interconnection foil with integrated copper conductor layer, on which the cells are electrically contacted using a conductive adhesive. Compared to a tabbed interconnection technology, the rear-side foil interconnection allows reduction of the module series resistance by using more interconnect metal (more cross-sectional area) and thereby reduces the cell to module FF loss. Also, the module manufacturing based on integrated back-foil can be done with higher yield and reduced interconnection-process-related stress, allowing use of (much) thinner cells and therefore offering additional cost reduction possibilities.So far, 2x2 cells IBC Mercury laminates successfully passed damp heat and thermal cycle tests as described by the IEC standard. Based on the same interconnection technology, a first 60-cell module is in preparation to monitor cell-to-module losses.

Recent developments in the process and design parameters of the Mercury cell have resulted in cell efficiencies up to 20.9% [7], which is an increase in efficiency of more than 1% absolute compared to the results that were reported previously [8]. One major process improvement contributing to this efficiency increase is related to the boron diffusion recipe used to create the FFE and rear emitter of our IBC Mercury cell. Effect of the boron diffusion recipe on the cell performance is discussed in the next section. In table I, the cell parameters of the best cell are shown. The I/V parameters were obtained in an in-house measurement using a class AAA solar simulator. The measurement chuck was especially designed for our Mercury cells, with current and voltage probes only contacting the module interconnection points, and a reflective but non-electrically-conductive chuck surface, representative for the situation in a module. The J_{sc} was corrected for spectral mismatch. The measurement was calibrated with a Fraunhofer-ISE-calibrated front-and-rear contact cell measured with a different chuck. Both for calibration and for IBC cell measurements, the chuck surface outside of the cell was masked with black tape, to avoid calibration errors due to variation in the chuck area and chuck reflectance.

Area [cm^2]	J_{sc} [mA/cm^2]	V_{oc} [mV]	FF [-]	Efficiency [%]
239	41.2	656	0.771	20.9

Table I. I/V parameters of the best IBC Mercury cell

Surface passivation of IBC cells is of high importance, firstly for high J_{sc} due to the long path lengths that minority carriers need to travel before being collected, and secondly to build up a substantial carrier density in order to achieve high V_{oc}. As mentioned earlier, the IBC Mercury cell is a gap-less IBC cell. Therefore, emitter and BSF diffused regions on the rear-side are in contact and this junction area should also be considered as sensitive area when it comes to passivation and resulting recombination. The next section focuses on this particular aspect of the Mercury cell: the pn-junction recombination and its impact on the cell performance.

III. PN-JUNCTION RECOMBINATION

1. Jo measurements of IBC structured surface

The surface passivation performance of the FFE, rear emitter and BSF areas can be extracted individually from Sinton quasi-steady state photoconductance (QSSPC) lifetime measurements on test structures with large-area (non-interdigitated) diffusions on each side. The characteristic recombination parameter J_0 can be determined from the slope of the (inverse, corrected for Auger recombination) lifetime curve as proposed by Kane and Swanson [9].

However, the J_0 determination of surfaces that are typical for an IBC cell, which incorporates emitter and BSF diffusion in an interdigitated pattern, is much more challenging than for a uniformly diffused surface. Both QSSPC or transient photoconductance measurements on these IBC structures are subject to artefacts that prohibit accurate evaluation of the lifetime and implied V_{oc}.

We can qualitatively describe these artefacts as follows: The photoconductance method relies on comparing the conductance of the sample in dark and under illumination, and changes of conductivity are assumed to be solely due to changes of carrier density. However, in dark conditions, the conductivity contribution of the emitter diffused fingers of the IBC structure to the inductive measurement is limited, since the pn-junctions between emitter and base and also between emitter and BSF fingers are not conductive, as sketched in Figure 3 (left side). Thus charges cannot move in and out of these diffused fingers and the conductivity is reduced.
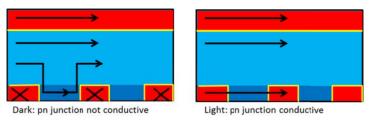

Dark: pn junction not conductive   Light: pn junction conductive

Fig. 3. *Schematic overview of conduction paths, e.g. for currents induced by the RF coil of the QSSPC tool, in dark and light conditions in a cross-section of an IBC Mercury cell. Red and blue correspond to the different polarities of the regions.*

However, under illumination the pn-junction starts to conduct as a function of light intensity (injection level) in the sample and the charges can move freely in and out of the diffused emitter (see Figure 3 right). This increased conductivity is measured by the induction coil. Since the photoconductance method attributes an increase in conductivity to the increased carrier concentration in the base of the sample, the enhanced conductivity due to the conducting pn-junctions causes the carrier density to be overestimated. This results in a sudden increase in apparent lifetime at light intensities that cause the junction to "switch on", leading to an overestimation of the implied V_{oc}. This effect on the lifetime curve of an IBC structured sample is shown in Figure 4, and was reported earlier as well [10].
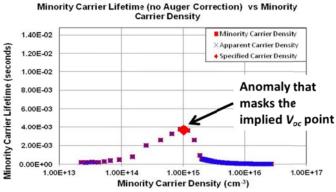

Fig. 4. *QSSPC lifetime curve of an IBC cell structure, showing the lifetime anomaly, leading to overestimated implied V_{oc} value.*

Despite this effect, the J_0 according to the method of Kane and Swanson can still be determined for IBC structures, as it is evaluated at very high injection levels ($\Delta n \gg 10^{15}$ cm-3) where the lifetime curve is not disturbed by the mentioned artefacts. The linear fit used for this method has a higher off-set but the slope is not affected and can therefore be used to characterize the surface recombination performance of the interdigitated structure.

The recombination parameter J_0 as determined by the Kane and Swanson method is related to the recombination characterized by an ideality factor n=1 for surfaces with one dominant carrier concentration such as diffused surfaces. This J_0 can be identified with the J_{01} parameter in a 2-diode equation for the cell. Shockley-Read-Hall recombination occurring in the bulk under high injection conditions or in a pn-junction has an ideality factor n=2 and is represented in the diode equation by the J_{02} parameter. When the method of Kane and Swanson is applied on photoconductance measurements of samples with homogeneous diffusions both bulk and pn-junction recombination will be reflected in the effective bulk lifetime [9].

As explained above, the effective bulk lifetime value is inaccessible when photoconductance measurements are carried out on IBC patterned samples. The IBC cell architecture that we work with entails a gap-less junction between BSF and emitter which could exhibit J_{02}-type recombination. As the total pn-junction length that meanders at the rear side of an IBC cell is relatively large, the recombination contribution of the gap-less emitter-BSF junction can have significant impact on the cell performance. In the next section, we present an alternative test method that enables quantification of the recombination activity at the pn-junctions and confirms that the J_0 determination from the slope of the QSSPC inverse lifetime curve is insensitive to this type of recombination, as expected.

2. Experimental set-up and method validation

In a first experiment, test structures were designed with interdigitated emitter and BSF areas on the rear side, and an FFE on the front side. The BSF and emitter fractions were kept constant, while the number of transitions, i.e. pn-junctions, on a test structure was varied between 5 and 20 junctions per centimetre as described in the next section. To illustrate the pn-junction recombination measurement possibilities and limitations, samples without any rear-side passivation were prepared in the first place. The passivation of the FFE was the same in all cases.

The surface passivation of the test structures without rear passivation was evaluated using the Sinton QSSPC lifetime measurements, which excludes the J_{02} and thus the pn-junction recombination contribution in the analysis. The resulting J_0 value is used to calculate the implied V_{oc} that would be reached if only the recombination at the highly doped surfaces would occur, by using the formula:

$$V_{OC} = \frac{kT}{q} \ln\left(\frac{J_{sc}}{J_{01}} + 1\right) \qquad (1)$$

Subsequently, the V_{oc} of the test structure was measured using the Sinton SunsV$_{oc}$ setup, without metallization grid. The V_{oc} measured in this case is affected by all sources of recombination.

Figure 5 shows the implied V_{oc} as calculated according to equation (1) based on J_0 values determined using the Sinton lifetime tester (red) and the V_{oc} measured in the SunsV$_{oc}$ measurement (blue). Both of these V_{oc} values are plotted as a function of the density of pn-junctions on the rear. Note that in both measurements the samples have no metallization. The contacting in the SunsV$_{oc}$ instrument was done by using metal pins directly in contact with the doped Si surfaces.
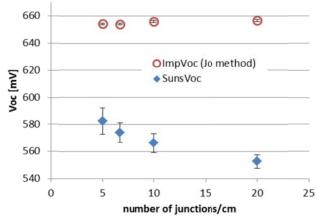

Fig. 5.   Implied V_{oc}, (derived from the surface J_0 determination in a Sinton lifetime tester, using equation 1) (red) and V_{oc} measured in a Sinton SunsV$_{oc}$ setup (blue) at 1 sun, as a function of pn-junction density, for an IBC test structure with no rear passivation.

Compared to the implied V_{oc} derived from surface J_0 determination in a Sinton lifetime tester, the SunsV$_{oc}$ measurement shows a dramatic V_{oc} drop as the junction density increases. The V_{oc} decreases from ~580 mV to ~550 mV as the number of junctions per cm increases from 5 to 20. The implied V_{oc} extracted from the J_0 determination in the photoconductance measurement instead shows an approximately constant value around ~655 mV, which is low because of the non-passivated rear side. From these results it is clear that the implied V_{oc} calculated from the Sinton lifetime tester data does not take into account the effects of junction recombination, as stated earlier. Therefore, the evaluation of the pn-junction recombination in a cell structure featuring an interdigitated diffused area such as the IBC Mercury cell requires, for instance, a SunsV$_{oc}$ measurement on a test structure including a variation of pn-junction density as proposed above.

3. PN-Junction recombination evaluation for the IBC Mercury cells

The same method based on the fabrication of test structures including variation of the pn-junction density was used to evaluate pn-junction recombination as a function of boron diffusion recipe. Following our current IBC Mercury process including front and rear side passivation, IBC cells and test structures were processed in parallel in two groups, each group corresponding to one boron diffusion recipe. In this case, fire-through metal contacts were also applied by screen-printing onto the test structure to ensure good contacting during the V_{oc} measurement. Metal fraction per diffused area was kept constant and is similar to the metal fraction used for an IBC Mercury cell. As a result, for each boron diffusion recipe, cells and their corresponding test structure were fabricated. A schematic of the four sub-cells with different junction density including the metallisation grid is shown in figure 6. Each sub-cell has a dimension of 19x38cm. A 6 inch wafer includes four rows of eight sub-cells. The eight sub-cells in one row are identical (one junction density).
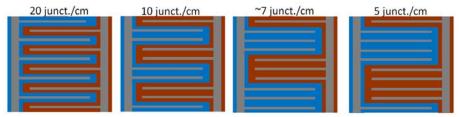

Fig. 6. Schematic of the 4 sub-cells with different junction density (5 to 20 junctions per centimetre). The blue and red areas are the boron and phosphorus-doped regions. The grey areas are the metallisation grid.

From the SunsV$_{oc}$ measurement, the V_{oc} and pseudo-FF are reported in figure 7 as a function of junction density. Due to suboptimal process parameters in other process steps used in this experiment, V_{oc} levels are below the recent best V_{oc} reported in the second section of this paper.
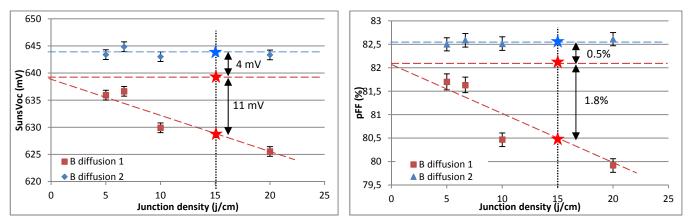

Fig. 7. V_{oc} and pseudo-FF dependence of IBC test structures as a function of pn-junction density. Data are shown for 2 boron diffusion recipes. Stars indicate the junction density of the Mercury cells in this publication.

While the V_{oc} (top chart) and pseudo-FF (bottom chart) trends as a function of the pn-junction density are constant for the test structure processed with the boron diffusion recipe 2, the test structure processed with the boron diffusion recipe 1 shows a significant drop in V_{oc} and pseudo-FF when the junction density increases. The trend can be assumed to be linear in a first approximation. By applying a linear fit, the decrease in V_{oc} and pseudo-FF can be estimated respectively at around 0.7mV and 0.1%abs loss per unit of junction density. Also, from the Y-intercept, it is possible to extrapolate the theoretical V_{oc} and pFF values in the absence of pn-junction. By comparing the Y-intercept of the SunsV$_{oc}$ curve in figure 7 of both boron diffusion recipes, a difference of 4 mV in V_{oc} is found. This difference matches with the difference in implied Voc measured in

the Sinton QSSPC lifetime tester which excludes J_{02} and thus the pn-junction recombination. Therefore Voc value at the Y-intercept of the

SunsVoc curve in figure 7 is representative for the Voc influenced by ideal recombination, i.e. recombination characterized by an ideality factor n=1, and by contact recombination. Following the rational further, it can be inferred that no other Jo2 recombination, such as in the emitter / base junction, has a significant contribution to the V_{oc} of the cell.

Based on these observations, the V_{oc} and pseudo-FF losses measured on the test structures were compared to the V_{oc} and pseudo-FF measured on the corresponding IBC mercury cells processed in parallel. Results are summarized in table II for both diffusion recipes. In the top part of table II, V_{oc} and pseudo-FF measured on the IBC cells are shown including the V_{oc} and pseudo-FF differences relative the cell processed with the boron diffusion recipe 2. In the bottom part of the table II, V_{oc} and pseudo-FF losses related to pn-junction recombination measured on the test structures are shown for a junction density equal to the junction density used for an IBC Mercury cell (15 junctions/cm). These losses therefore correspond to the difference between the value at the Y-intercept (junction density=0) and the value at 15 junction/cm junction density as marked on the plots in figure 7 (delta V_{oc} between the 2 red stars).

The lower V_{oc} at the Y-intercept of the "boron diffusion 1" group compared to the "boron diffusion 2" group is related to J_{01}-type recombination and could differ due to differences in, e.g., surface passivation or Auger recombination. This V_{oc} difference, reported in table II and marked in the plots of figure 7 (delta V_{oc} between the blue star and the upper red star), also contributes to the overall V_{oc} loss measured on the cells of the "boron diffusion 1" group relative to the "boron diffusion 2" group.

	Average V_{oc} (mV)	Average Pseudo-FF (%)
IBC Cells *(7 cells per diffusion recipe)*		
Cell - B diff 1	627	79.2
Cell - B diff 2	643	80.7
Total losses at cell level of B diff 1 group, relative to B diff 2 group	**16**	**1.5**
Test structures *(16 sub-cells per diffusion recipe)*		
pn-junction related losses - B diff 1 group	11	1.8
pn-junction related losses - B diff 2 group	0	0
Ideal recombination related losses of B diff 2 group, relative to B diff 1 group	4	0.5
Total losses at test structure level of B diff 1 group, relative to B diff 2 group	**15**	**2.3**

Table II. V_{oc} and pseudo-FF losses measured on IBC cells and on their corresponding test structures. V_{oc} and pseudo-FF losses of the "boron diffusion group 1" are calculated at cell level and test structure level relative to the V_{oc} and pseudo-FF of the cells and test structures of the "boron diffusion group 2".

As shown in table II, the V_{oc} loss of the "boron diffusion 1" group relative to the "boron diffusion 2" group measured at cell level is in fair agreement with the total V_{oc} loss calculated on the test structures. However, the pseudo-FF loss measured on test structures is slightly higher than the pseudo-FF loss measured on the cells. Also, the absolute pseudo-FF value extrapolated from the test structures at the 15 junction/cm mark is higher than the pseudo-FF measured on its corresponding IBC Mercury cell. This discrepancy in the pseudo-FF results is for the moment not well-understood and needs further investigation. One possible explanation could be related to the non-uniformity of the pn-junction recombination activity across the cell, result of the non-uniformity of some process steps. The test structure design includes several sub-cells, with different pn-junction densities, on one wafer. Therefore, in contrast to an I/V measurement performed on a cell influenced by the complete area of the cell, the SunsV$_{oc}$ measurement performed on the test structures remains rather local.

Despite this slight divergence of the pseudo-FF, this method allows us to reliably estimate the effect of the pn-junction recombination activities on the V_{oc} of our IBC Mercury cell. By processing these test structures in parallel to IBC cells, which only involves a simple change of pattern, we could compare several boron diffusion recipes and correlate their performance differences with the recombination activity present at the pn-junction. Detailed correlation between boron and phosphorus doping profile (e.g. doping concentration or junction depth) and pn-junction recombination activity is still to be investigated. Thanks to these test structures, any process modification made to our IBC Mercury cell (such as diffusion patterning method, diffusion recipes, passivation schemes…) can be monitored and optimised with respect to their impact on the pn-junction recombination activity and V_{oc} of the cell. The boron diffusion recipe 2 was selected to manufacture our current most efficient IBC Mercury cell presented in the previous section.

IV. FURTHER OPTIMISATION OF THE CELL PROCESS

Table V illustrates the potential of three scenarios for increasing cell efficiency. The scenarios are based on 2-D Quokka [11] simulations on a cross-section of a single unit cell (indicated by the dashed box in Figure 1). Tables III and IV give details on some key input parameters of the simulations. In these scenarios, several BSF and FFE diffusions and different metallization techniques are considered. The resistance of the metal grid (fingers and busbars) are calculated separately, and included as a lumped series resistance in the 2-D Quokka simulation. We consider for instance standard fire-through (FT) and gentler non-fire-through (non-FT) screen printed metallization, and metallization deposited by physical vapor deposition (PVD). A FT metallization can penetrate a significant distance (a typical number can be upto ~200 nm) into the diffusion during firing, resulting in high recombination, especially on light diffusions.

The difference between PVD and non-FT metallization is not only in the J_0 values (see Table III), but also in the shape of the contacts. Both require opening of the dielectric prior to application of the metallization. However, the non-FT metallization is assumed to be screen printed, as (narrow) fingers. The PVD metallization is applied nearly full-area, with suitable gaps isolating contacts of opposite polarity.

We considered two geometries: a geometry with BSF and emitter width of 250 and 800 μm respectively ("high efficiency", abbreviated as HE), and one with both BSF and emitter having a width of 1000 μm ("easy manufacturing", abbreviated as EM). The different geometries and scenarios result in different metal coverages, as indicated in Table IV.

scenario	BSF		emitter	
	J_0 (non-c)	J_0 (c)	J_0 (non-c)	J_0 (c)
	fA/cm^2	fA/cm^2	fA/cm^2	fA/cm^2
A	230	1200	57	2000
B	72	500	57	450
C	72	500	57	450

Table III. J_0 values applied for contacted (c) and non-contacted (non-c) diffusions

scenario	BSF contact		emitter contact	
	HE	EM	HE	EM
	%	%	%	%
A	7.6	4.0	4.0	3.3
B	7.6	4.0	4.0	3.3
C	2.9	1.5	1.5	1.5

Table IV. Metal contact fractions values for different scenarios and geometries

For our current cell, which features the BSF and metallization scheme according to scenario A, we achieved the cell efficiency of 20.9% on a full 6 inch wafer, as presented in Table I. However, the difference between the parameters of this cell and of the simulation of scenario A (as shown in Table V) is in the FF, which should be improved significantly and the reasons for its reduction are being investigated.

For the other two scenarios we employed a lighter BSF, which is more difficult to contact using our standard fire-through metallization, but should be well contactable using non-FT metallization in scenario B and PVD metallization in scenario C. The emitter and BSF contact recombination in both scenario B and C were assumed to decrease from 2000 to 450 fA/cm^2 (emitter) and from 1200 to 500 fA/cm^2 (BSF), and will therefore boost the efficiency potential to 22.6% for scenario B and to 23.1% for scenario C. The optional use of a lighter FFE in scenario C is expected to give an additional 0.2% absolute increase in efficiency to 23.3% (not shown). The sheet resistance of this lighter FFE was 150 Ωcm while the associated J_0 was set to 30 fA/cm^2. The complete set of I/V parameters that resulted from HE scenario A, B and C is listed in Table VI. It can be seen that only slightly lower efficiencies are expected for the EM geometry, thanks to the presence of the FFE and the pumping effect, which mitigates the electrical shading to a large extent.

scenario	BSF diffusion	metal	Efficiency [%]
A	heavy	FT	21.8
B	light	non-FT	22.6
C	light	PVD	23.1

Table V. Efficiency potential of mercury IBC cell in different scenarios (R_{bulk}=5 Ωcm, HE geometry)

scenario	HE				EM
	J_{sc}	V_{oc}	FF	η	η
	mA/cm^2	mV	%	%	%
A	41.2	656	80.8	21.8	21.5
B	41.3	672	81.6	22.6	22.4
C	41.4	680	82.3	23.1	22.9

Table VI. I/V parameters of mercury IBC cell in different scenarios (R_{bulk}=5 Ω.cm)

V. CONCLUSION

We developed an industrial process to manufacture IBC Mercury cells featuring a front floating emitter on 6 inch n-type mono-crystalline Czochralski (Cz) silicon wafers. In the course of the process optimisation, we investigated a method to

determine the recombination losses due to the pn-junctions in Mercury IBC cells and their impact on the performance of these cells. Based on the use of dedicated test structures and from a linear approximation of the losses associated with the number of pn-junctions, we could consistently quantify the effect of pn-junction recombination on the V_{oc} of the cell. For a specific case in which the boron diffusion was varied, we could correlate the recombination activity at the pn-junction with different emitter boron diffusion recipes. By using the boron diffusion recipe that result in no noticeable pn-junction recombination and with additional optimisation of our industrial process, efficiency of our IBC Mercury cells could be improved by more than 1% absolute, leading to cell efficiency close to 21%. The ECN module manufacturing technology based on integrated back-foil will soon be used to make the first 60-cells IBC Mercury module. From 2-D Quokka simulation results, we foresee that 23% Mercury IBC cells are within reach upon changing the BSF diffusion to a lighter profile, and changing the metallization to less recombination-inducing alternatives.

VI.   ACKNOWLEDGEMENT

VII.   REFERENCES

[1]   http://www.itrpv.net/Reports/Downloads/ - ITRPV_2015_Roadmap_Results_2014_150428.pdf – page 27
[2]   M. Hermle et al., "Shading Effects in Back-Junction Back-Contacted Silicon Solar Cells", *Proc. 33rd IEEE Photovoltaic Specialists Conference*, St. Diego, CA, (2008).
[3]   I. Cesar, N. Guillevin, A.R. Burgers, A.A. Mewe, M. Koppes, J. Anker, L.J. Geerligs, and A.W. Weeber, "Mercury: a back junction back contact front floating emitter cell with novel design for high efficiency and simplified processing" *Energy Procedia,* vol 55 2014, p. 633
[4]   Müller et al., "Back-junction back-contact n-type silicon solar cell with diffused boron emitter locally blocked by implanted phosphorus", *Applied Physics Letters, 105, 103503* (2014)
[5]   R. Kopecek et al. "c-Si n-Type Technology: Break Through or Break Down?", *4th Silicon PV conference,* Den Bosh, The Netherlands (2014).
[6]   I. Bennett, presented at *MWT workshop*, 2010, Amsterdam
[7]   P. Spinelli, N. Guillevin, T. Burgers, A. Mewe, A. Vlooswijk, B. Geerligs, and I. Cesar, "Front-floating emitter voltage mapping of IBC Mercury cells", *SiliconPV*, 2015, Constance, to be published.
[8]   I. Cesar, N. Guillevin, A.R. Burgers, A.A. Mewe, E.E. Bende, V. Rosca, B. van Aken, M. Koppes, J. Anker, L.J. Geerligs, and A.W. Weeber, "Mercury: a novel design for a back junction back contact cell with front floating emitter for high efficiency and simplified processing" *Proc. EUPVSEC,* 2014, Amsterdam
[9]   D.E. Kane and R.M. Swanson, "Measurement of the emitter saturation current by a contactless photoconductivity method", *Proc. 18th IEEE PVSC*, 1985, p. 578-581
[10]   M. Juhl, C. Chan, M.D. Abbott, and T. Trupke, "Anomalously high lifetimes measured by quasi-steady-state photoconductance in advanced solar cell structures", *Applied Physics Letters* 103, 2013, 243902
[11]   A. Fell, "A free and fast 3D/2D solar cell simulator featuring conductive boundary and quasi-neutrality approximations," *IEEE Transactions on Electron Devices*, Vol 60 (2), pp. 733–738, 2012.